scientific reports

OPEN

Cyclophilin D suppresses colorectal cancer progression through the activation of an autophagy-mediated apoptotic pathway

Ling Zhang[1], Yi Liu[2], Ruiqi Liu[3], Wenjun Wang[4]✉ & Ruiji Li[5]✉

Colorectal cancer (CRC) remains a leading gastrointestinal malignancy and lacks effective adjuvant therapies. Cyclophilin D (CypD), a mitochondrial matrix protein, has a controversial role in tumorigenesis. While prior studies suggest a CypD-CRC link, its precise function and mechanisms remain undefined. Here we clarify whether CypD acts as a driver or suppressor of CRC and explore its therapeutic implications. Using RT-qPCR, Western blotting, and immunofluorescence, we confirmed significant CypD downregulation in CRC tissues/cells versus non-malignant controls. Through in vitro (CCK-8, colony formation, transwell migration, spheroid formation, apoptosis, and autophagy assays) and in vivo tumor xenograft experiments with CypD-knockdown/overexpressing CRC cells (DLD1 and RKO), knocking down CypD promoted, whereas its overexpression inhibited, malignant phenotypes (proliferation, migration, self-renewal, tumorigenicity). Mechanistically, CypD activated protective autophagy and cell apoptosis, with autophagy inhibitor chloroquine reversing this effect. Critically, knocking down CypD attenuated the anti-CRC efficacy of 5-fluorouracil/epigallocatechin-3-gallate combination therapy, whereas its overexpression enhanced therapeutic response. This study provides the first definitive evidence that CypD functions as a tumour suppressor via autophagy-apoptosis crosstalk. Low CypD expression may serve as a biomarker for poor treatment response. Enhancing CypD activity represents a promising strategy to augment existing CRC treatments.

Keywords Cyclophilin D, Colorectal cancer, Malignant phenotype, Autophagy, Apoptosis

According to the latest statistics, colorectal cancer (CRC) accounted for over 1.9 million new cases (ranking third) and 904,000 deaths (ranking second) worldwide in 2022[1]. While current treatments (e.g., surgery, chemotherapy, and immunotherapy) have somewhat extended patient survival, CRC management remains hindered by challenges such as low early-stage diagnosis rates and high metastatic propensity[2]. Molecular-targeted therapies, while effective in specific gene-mutated subtypes (e.g., *BRAF* V600E mutation and *HER2* amplification), have limited patient coverage and drug-resistance issues[3]. Consequently, identifying novel predictive biomarkers and optimizing combination therapies are key to breaking current treatment limitations in CRC.

Mitochondria are central regulators of cancer cell survival, metabolism, and apoptosis, making them attractive therapeutic targets for cancer treatment. Dysregulated mitochondrial function is a hallmark of cancer, and targeting mitochondrial components or pathways has emerged as a promising strategy to inhibit tumor progression and enhance chemosensitivity. Cyclophilin D (CypD), encoded by the gene *Ppif*, is a critical mitochondrial matrix protein that modulates mitochondrial permeability transition (mPT). Through positive regulation of mPT, CypD plays a pivotal role in apoptosis, oxidative stress, and energy metabolism[4]. Emerging evidence highlights its functional significance in ischemic-reperfusion injury, neurodegenerative disorders, and oxidative stress-related pathologies[5–7], yet its implications in tumorigenesis remain contentious[8]. While some studies have proposed that CypD may suppress tumor growth by activating pro-apoptotic pathways[9–11], conflicting reports have associated increased CypD expression with enhanced chemoresistance and aggressiveness in cancer cells[12,13]. Notably, CypD knockdown has been shown to attenuate cytotoxicity induced

[1]School of Nursing, Jining Medical University, Jining 272067, Shandong, China. [2]School of Public Health, North China University of Science and Technology, Tangshan 063210, Hebei, China. [3]Biobank, Xi'an People's Hospital (Xi'an Fourth Hospital), Xi'an 710004, Shaanxi, China. [4]Weifang Nursing Vocational College, Qingzhou 262500, Shandong, China. [5]School of Pharmacy, Jining Medical University, Rizhao 276826, Shandong, China. ✉email: wwjun1973@163.com; li-ruiji@mail.jnmc.edu.cn

by multiple anticancer agents in CRC cells[14–16], yet its specific function and potential mechanisms have not been systematically elucidated.

5-Fluorouracil (5-FU) serves as a cornerstone of multiple CRC chemotherapy regimens, though its clinical efficacy is severely compromised by the emergence of drug resistance[17]. Chemosensitizers enhance the cytotoxicity and antitumor activity of 5-FU by optimizing its intracellular metabolic pathways. For example, 5-FU combined with gambogenic acid has been shown to synergistically induce apoptosis in lung cancer cells via a mitochondrial-targeted pathway, which accompanied by CypD upregulation[18]. Similarly, epigallocatechin-3-gallate (EGCG), a major bioactive component of green tea, has also been identified as a potential chemosensitizer for 5-FU due to its antioxidant, antitumor, and low-toxicity profile. Preclinical studies confirm that EGCG significantly enhances 5-FU sensitivity in various malignancies, including gastric, breast, and colorectal cancers, with documented mechanisms underlying this synergy[19–21]. Moreover, EGCG could alleviate mitochondrial damage by directly binding to CypD and blocking the CypD-partner interactions[22]. However, the potential role of CypD in mediating the synergistic antitumor effects of EGCG and 5-FU in CRC remains unexplored. We hypothesized that CypD may act as a key mediator of this combinatorial efficacy. If confirmed, CypD could emerge as a molecular target for potentiating the combinatorial antitumor efficacy of EGCG and 5-FU against CRC.

This study investigated the expression profiles of CypD, a key mitochondrial regulator, in CRC clinical samples and established human CRC cell lines. By generating stable CypD knockdown and overexpression CRC cell models, we subsequently linked CypD functional modulation to cellular malignant phenotypes and in vivo tumorigenicity. Furthermore, we implemented the combined intervention strategy of the natural compound EGCG with the chemotherapeutic agent 5-FU, initially revealing the role of CypD as a key regulatory node in this synergistic therapy. These findings provide a theoretical basis for enhancing chemotherapeutic efficacy and developing new synergistic regimens targeting mitochondrial metabolism in CRC treatment.

Results

Expression of CypD in CRC tissues and cell lines

Bioinformatics analysis of TCGA dataset revealed significantly elevated CRC tumor-specific *Ppif* mRNA expression in T1-stage compared to T4-stage ($P<0.05$; Fig. 1a). As shown in Fig. 1b, CypD demonstrated promising diagnostic efficacy for CRC (AUC = 0.849, 95%CI = 0.808–0.890), suggesting its potential as a

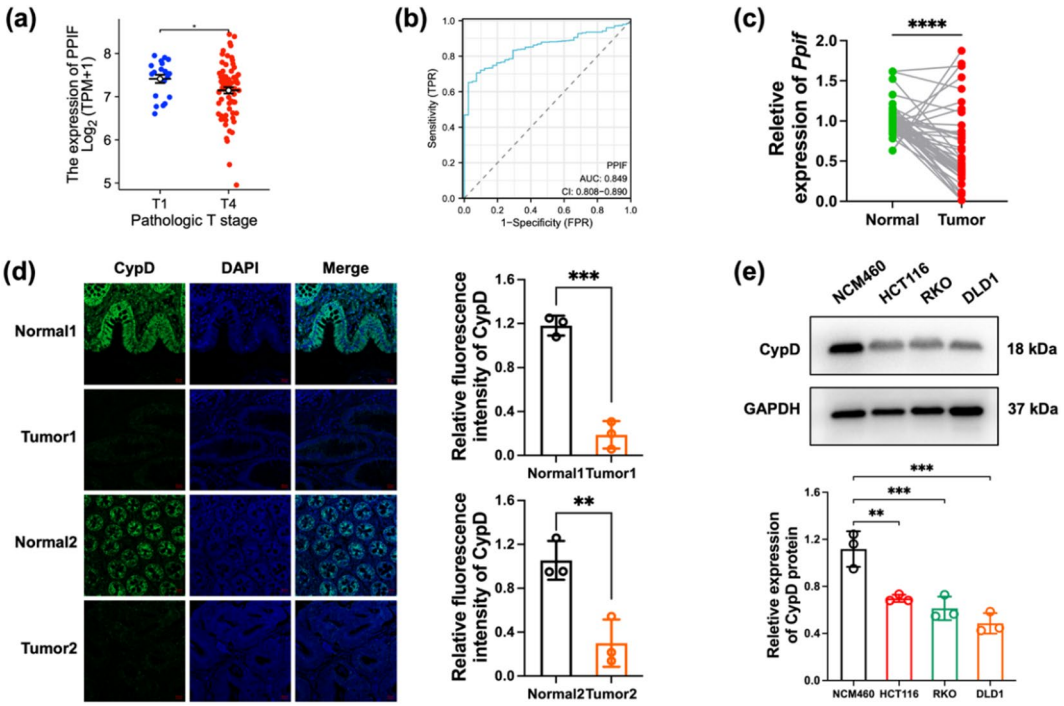

Fig. 1. Reduced CypD expression in CRC tumors and cell lines. (**a**) Differences in CypD protein expression between T1 and T4 CRC patients from the TCGA database (Mann-Whitney *U* test). (**b**) ROC curve analysis demonstrating CypD's diagnostic performance for CRC. (**c**) *Ppif* gene expression in cancerous and para-carcinoma tissues of 11 CRC patients detected by RT-qPCR (paired *t*-test). (**d**) CypD protein levels in cancerous and para-carcinoma tissues of two additional CRC patients assessed by IF staining (scale bar = 20 μm; independent-samples *t*-test). (**e**) Comparison of CypD expression in human normal colorectal epithelial cells (NCM460) and three CRC cell lines (DLD-1, RKO, HCT116) by Western blotting (one-way ANOVA followed by Tukey's HSD test). All Western blots were derived from physically cut membrane strips, and lanes non-adjacent or from different gels were separated by white space. * $P<0.05$, ** $P<0.01$, *** $P<0.001$, and **** $P<0.0001$.

candidate biomarker. To further investigate CypD's role, we compared its mRNA and protein expression between cancerous and para-carcinoma tissues using RT-qPCR and IF staining. It was found that CRC tissues exhibited significantly reduced *Ppif* mRNA levels compared to para-carcinoma tissues ($P < 0.0001$; Fig. 1c). Consistently, CypD protein levels were lower in CRC tumor tissues (weakly positive) than in para-carcinoma tissues ($P < 0.01$; Fig. 1d). CypD protein expression was further detected in three human CRC cell lines (HCT116, RKO, DLD1) and immortalized human colorectal epithelial cell (NCM460). As expected, all three CRC cell lines showed significantly reduced CypD expression compared to NCM460 cell (all $P < 0.01$; Fig. 1e). Notably, DLD1 and RKO cells exhibited the most pronounced downregulation (both $P < 0.001$) and were thus selected for subsequent studies.

Effect of CypD knockdown on biological behavior of CRC cells

To elucidate the regulatory role of CypD in CRC cells, stable CypD-knockdown and CypD-overexpressing cell models were established in DLD1 and RKO cell. As shown in Fig. 2a, *Ppif* gene expression was significantly reduced in sh CypD group compared to sh NC group (both $P < 0.001$). Conversely, cells in Ad CypD group showed marked upregulation of *Ppif* gene levels relative to Ad vector group (both $P < 0.0001$). Western blotting analysis further confirmed effective modulation of CypD expression in these cell lines (Fig. 2b), indicating successful construction of CRC cell models with stable intervention in CypD expression.

Subsequently, the impact of CypD on malignant biological behaviors of CRC cells was analyzed using the constructed cell lines. CCK-8 assays revealed that CypD knockdown in DLD1 and RKO cells enhanced proliferation in a time-dependent manner compared to sh NC group (both $P < 0.05$), while CypD overexpression reduced proliferation versus Ad vector group (both $P < 0.05$) (Fig. 2c). Although RKO exhibited a larger fold-change in CypD mRNA and protein after transfection (Fig. 2b), the corresponding alteration in proliferative capacity (Fig. 2c) was more pronounced in DLD-1. Given that DLD1 cells harbor *KRAS* G13D mutation and PI3K pathway activation, while RKO cells exhibit microsatellite instability (MSI) and *BRAF* V600E mutation. These genetic differences might underlie the differential responsiveness to CypD modulation[23]. In addition, colony formation assays demonstrated 1.79-fold and 1.67-fold increases in colony numbers for CypD-knockdown DLD1 and RKO cells respectively (both $P < 0.05$). Following CypD overexpression, colony formation decreased by 36.1% and 76% in DLD1 and RKO cells respectively (both $P < 0.05$; Fig. 2d). Transwell migration assays further revealed that knocking down CypD increased cell migration rates to 2.32-fold and 2.33-fold of sh NC groups after 48-hour culture (both $P < 0.001$), while CypD overexpression reduced migration by 20.7% and 75.4% in DLD1 and RKO cells respectively after 72-hour culture (both $P < 0.01$; Fig. 2e). Spheroid formation assays were conducted to assess self-renewal capacity, revealing 3.87-fold and 2.29-fold increases in spheroid numbers for DLD1 and RKO cells in sh CypD groups after 10-day suspension culture (both $P < 0.05$; Fig. 2f). Conversely, CypD overexpression decreased spheroid formation by 76.2% and 83% in DLD1 and RKO cells respectively compared to Ad vector groups after 14-day culture (both $P < 0.05$). Collectively, these results demonstrate that CypD depletion promotes malignant phenotypes in CRC cells, whereas its overexpression exerts opposing effects.

Effect of intervening CypD expression on subcutaneous tumor growth in nude mice

To further investigate the in vivo impact of CypD modulation on CRC tumorigenesis, DLD1 cells were subcutaneously inoculated into BALB/c nude mice to establish tumor xenograft models. As shown in Fig. 3a, knocking down CypD significantly accelerated tumor growth starting from week 2 post-inoculation, whereas CypD overexpression produced the opposite effect (both $P < 0.01$). Consistently, tumors in the sh CypD group exhibited marked increases in both volume and weight compared to the sh NC group, while Ad CypD group showed significant reductions in these parameters relative to Ad vector group (both $P < 0.05$; Fig. 3b). The individual tumor measurements (width and length) for each animal at each time point, tumor weights on day 23, and animal weights on day 23 are presented in Tables S1, S2, and S3, respectively. As Ki67 expression indicates tumor cell proliferation activity, IHC staining was used to evaluate the effect of CypD expression modulation on CRC tumor growth. As expected, knocking down CypD enhanced Ki67-positive staining intensity in tumor tissues, whereas CypD overexpression suppressed Ki67 expression (Fig. 3c). It is important to note that while the extent of CypD knockdown in Fig. 2B and the observed effects on cell growth in Fig. 3C may appear discordant, this discrepancy likely arises from the fact that Fig. 2B reflects short-term CypD depletion in DLD1 cells under controlled in vitro conditions, whereas Fig. 3C involves prolonged dynamic interactions between tumor cells and the microenvironment (e.g., hypoxia and immune responses). Additionally, such differences may stem from the distinct microenvironmental contexts between 2D monolayer culture in vitro and 3D growth in vivo, including variations in nutrient availability. Collectively, these factors are likely key contributors to the observed differences in basal growth rates of DLD1 cells between in vitro and in vivo experimental settings. Moreover, western blotting analysis of tumor lysates confirmed reduced CypD protein expression in sh CypD group and elevated expression in Ad CypD group compared to respective controls (Fig. 3d). These results suggest that CypD expression modulation significantly affects CRC tumor growth in vivo, with CypD upregulation effectively inhibiting tumor progression.

Inhibition of autophagy weakens the promotion of CypD on the mitochondrial apoptotic pathway in CRC cells

Previous studies have found that CypD can indirectly participate in the apoptosis of CRC tumor cells[14], and cell apoptosis often leads to reduced cell proliferation. So, here, Western blotting was used to check if CypD affects cell apoptosis. As shown in Fig. 4a and b, compared to the sh NC group, the sh CypD group had higher Bcl-2 expression ($P < 0.05$) but lower Bax and Cleaved-Caspase3 expression (both $P < 0.001$). Conversely, CypD overexpression significantly decreased Bcl-2 expression ($P < 0.05$) while markedly increasing Bax and cleaved-

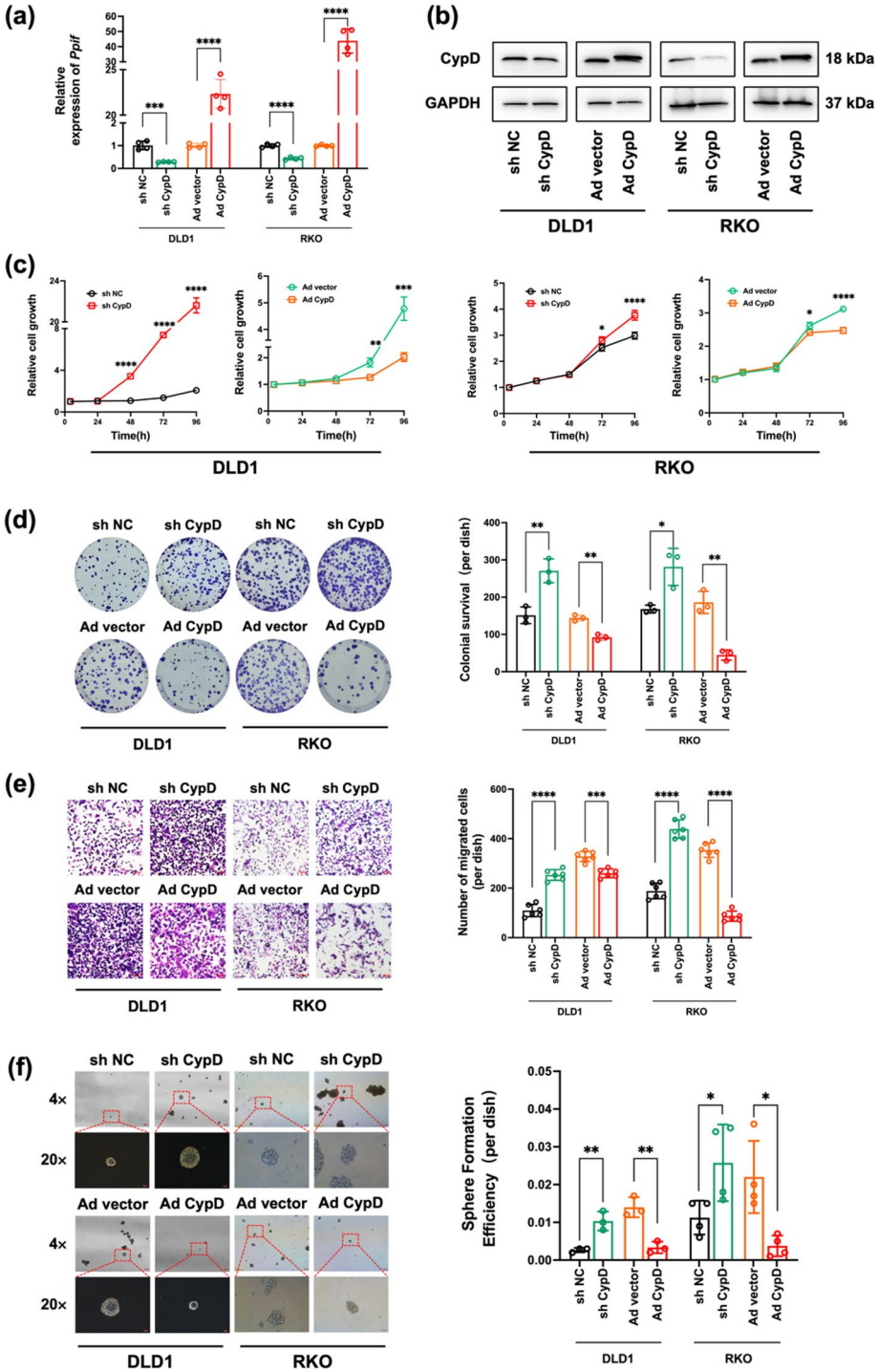

Fig. 2. Modulation of CypD expression affected CRC cell proliferation, migration, and self-renewal capacity. (**a**–**b**) Transfection efficiency was evaluated using RT-qPCR (one-way ANOVA followed by Tukey's HSD test) and Western blotting. Samples were collected on day 11–15 post-infection. All Western blots were derived from physically cut membrane strips, and lanes non-adjacent or from different gels were separated by white space. (**c**) CCK-8 assays were performed to assess changes in proliferative capacity of DLD-1 and RKO cells following CypD modulation (two-way ANOVA followed by Bonferroni-corrected *t*-test). (**d**) Colony formation assays were conducted to determine the effects of CypD intervention on CRC cell clonogenicity (one-way ANOVA followed by Tukey's HSD test). (**e**) Transwell migration assays analyzed alterations in migratory capacity of DLD-1 and RKO cells after CypD modulation (scale bar = 100 μm; one-way ANOVA followed by Tukey's HSD test). (**f**) Spheroid formation assays evaluated the impact of CypD expression changes on CRC cell self-renewal potential (scale bar = 200 μm and 50 μm; one-way ANOVA followed by Tukey's HSD test). * $P<0.05$, ** $P<0.01$, *** $P<0.001$, and **** $P<0.0001$.

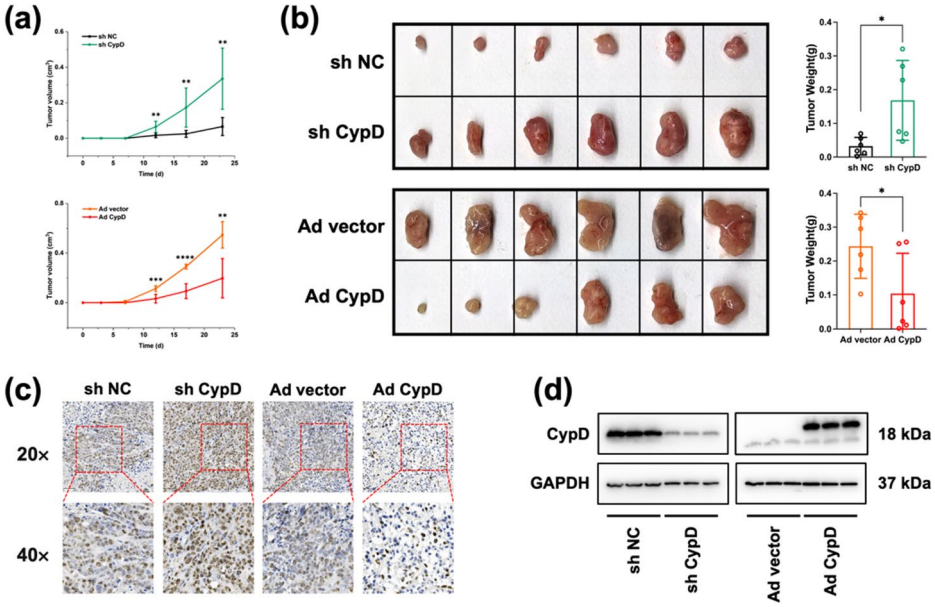

Fig. 3. Modulation of CypD expression affected growth of subcutaneous xenograft tumors in nude mice. (**a**) Tumor growth curves for each group following CypD intervention (measured on days 0, 3, 7, 12, 17, and 23) (two-way ANOVA followed by Bonferroni-corrected *t*-test). (**b**) Representative images and semi-quantitative analysis of tumor weight changes in subcutaneous xenografts harvested on day 23 (independent-samples *t*-test). (**c**) Representative IHC staining images for Ki67 in subcutaneous tumor (scale bar = 50 μm and 30 μm). (**d**) CypD protein expression in tumor lysates was evaluated using Western blotting analysis. All Western blots were derived from physically cut membrane strips, and lanes non-adjacent or from different gels were separated by white space. * $P<0.05$, ** $P<0.01$, *** $P<0.001$, and **** $P<0.0001$.

caspase 3 levels compared to Ad vector group (both $P < 0.0001$). These findings suggest that CypD may influence DLD-1 cell survival through regulation of intrinsic apoptotic pathways.

Additionally, studies have shown that excessive autophagy activation can significantly induce apoptosis[24]. We further investigated the effects of CypD modulation on autophagic activity in DLD-1 cells using Western blotting analysis. As shown in Fig. 4a and c, knocking down CypD significantly increased p62 protein ($P < 0.001$) while concomitantly reducing ATG7, ATG5, and LC3-II expression (all $P < 0.01$). Conversely, CypD overexpression produced inverse trends in these autophagy-related proteins (all $P < 0.01$). This suggests that CypD can induce LC3-I/LC3-II conversion to activate autophagy in DLD-1 cells.

Chloroquine (CQ), a commonly used autophagy inhibitor, suppresses autophagy by blocking autophagolysosome fusion and degradation[25]. Subsequently, we treated the Ad vector group and Ad CypD group with CQ to verify the dependency of CypD's biological effects on autophagy. As shown in Fig. 4d and e, 24 h of CQ treatment reduced Bax, Cleaved-Caspase 3, and LC3-II levels, and attenuated CypD overexpression-induced elevation of these proteins (all $P < 0.01$). Critically, no significant differences in the expression of these autophagic and apoptotic markers were observed between the CQ-Ad vector group and CQ-Ad CypD group. Notably, CQ treatment significantly decreased the LC3-II/I ratio in both groups, which appears contradictory to the classical effect of CQ (typically causing LC3-II accumulation). This phenomenon may be attributed to negative feedback regulation of autophagy initiation. Specifically, CypD promoted LC3-II generation by activating autophagy initiation (as supported by elevated ATG5/ATG7), while CQ blocked autophagosome degradation and might trigger downstream negative feedback (e.g., possibly inhibiting ULK1 complex activity), thereby reducing LC3-I lipidation to LC3-II. This "net reduction" of LC3-II/I ratio further confirms that CypD's ability to sustain autophagy activation relies on intact autophagic flux. In other words, if CypD functioned independently of intact autophagic flux, LC3-II would accumulate due to unimpaired generation and blocked degradation. Collectively, these results demonstrate that CypD modulates DLD-1 cell apoptosis in an autophagic flux-dependent manner, with CypD may acting as a positive regulator of complete autophagic flux.

CypD participates in the synergistic inhibition of EGCG and 5-FU on the biological behavior of CRC cells

To establish optimal treatment parameters, DLD-1 cells were exposed to varying concentrations of EGCG and 5-FU, with cell viability assessed at multiple time points using CCK-8 assays. As shown in Fig. 5a, both EGCG and 5-FU treatments demonstrated time-dependent inhibition of proliferation compared to the NC group. At 48 h of treatment, IC_{50} values were determined as 200 μM for EGCG ($P < 0.05$) and 150 μM for 5-FU ($P < 0.001$). Following parameter validation, cells were treated with EGCG, 5-FU, or their combination. Consistent with previous findings[21], all three regimens significantly reduced colony formation capacity (Fig. 5b), with EGCG treatment showing a significant reduction compared to the NC group ($P < 0.0001$). Notably, monotherapy

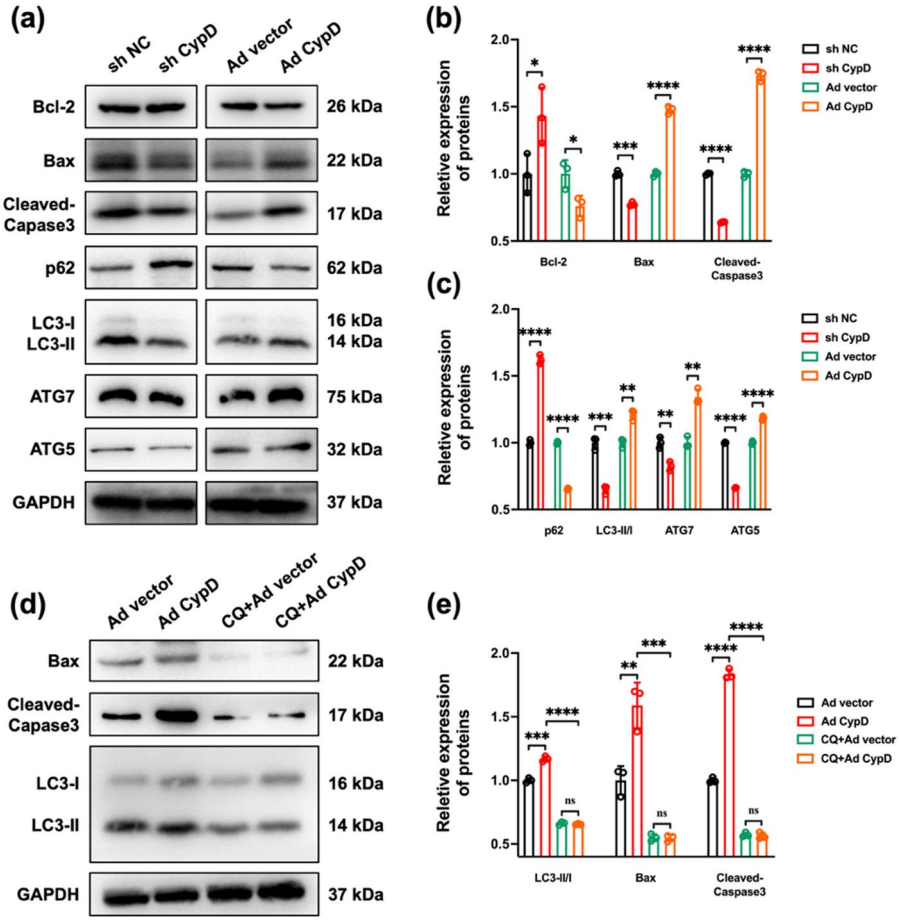

Fig. 4. CypD promoted apoptosis pathway activation in DLD1 cells via autophagy regulation. (**a**) Western blotting analysis of apoptosis- and autophagy-related protein expression in DLD1 cells across experimental groups. All Western blots were derived from physically cut membrane strips, and lanes non-adjacent or from different gels were separated by white space. (**b**) Semi-quantitative analysis of apoptosis-related proteins (Bcl-2, Bax, and Cleaved-Caspase 3) following CypD knockdown or overexpression (independent-samples *t*-test). (**c**) Semi-quantitative assessment of autophagy-related proteins (p62, ATG7, ATG5, and LC3) expression under CypD modulation (independent-samples *t*-test). (**d**) Protein expression of Bax, Cleaved-Caspase 3, and LC3 in Ad vector and Ad CypD groups with or without autophagy inhibitor CQ treatment. All Western blots were derived from physically cut membrane strips, and lanes non-adjacent or from different gels were separated by white space. (**e**) Semi-quantitative analysis of corresponding protein expression from part d (one-way ANOVA followed by Tukey's HSD test). * $P<0.05$, ** $P<0.01$, *** $P<0.001$, and **** $P<0.0001$.

with 5-FU produced 5.64-fold more colonies than the combination group ($P < 0.05$). Migration assays revealed marked suppression of cell motility in all treatment groups compared to the NC group (Fig. 5c), with 5-FU monotherapy showing 7.57-fold higher migration compared to the combination ($P < 0.001$). Sphere formation assays also demonstrated that EGCG or 5-FU treatment alone reduced the number of spheres formed by DLD-1 cells, with combined treatment further decreasing the number to 33.9% of that in the 5-FU group ($P < 0.01$) (Fig. 5d). These results indicate that EGCG effectively enhances the inhibitory effects of 5-FU on the biological behavior of DLD-1 cells.

Next, to verify if CypD is involved in the synergistic inhibitory effects of EGCG and 5-FU on CRC cells, we assessed CypD expression via RT-qPCR and Western blotting. As shown in Fig. 5e and f, compared to the NC group, CypD mRNA and protein expression were upregulated in all treatment groups (all $P<0.05$), with the combined treatment group showing 1.18-fold and 1.23-fold higher expression than the 5-FU group (both $P<0.05$). Additionally, knocking down CypD reversed the inhibitory effects of combined treatment on DLD-1 cells, as evidenced by significantly improved cell viability (Fig. 5g), migration (Fig. 5h), and sphere—forming ability (Fig. 5i) (all $P<0.0001$). Conversely, CypD overexpression augmented the synergistic inhibitory effects of the combination regimen (Fig. 5g to i) (all $P<0.01$). This suggests that CypD may play a key role in EGCG-induced the sensitivity of CRC cells to 5-FU, with the underlying mechanisms warranting further study.

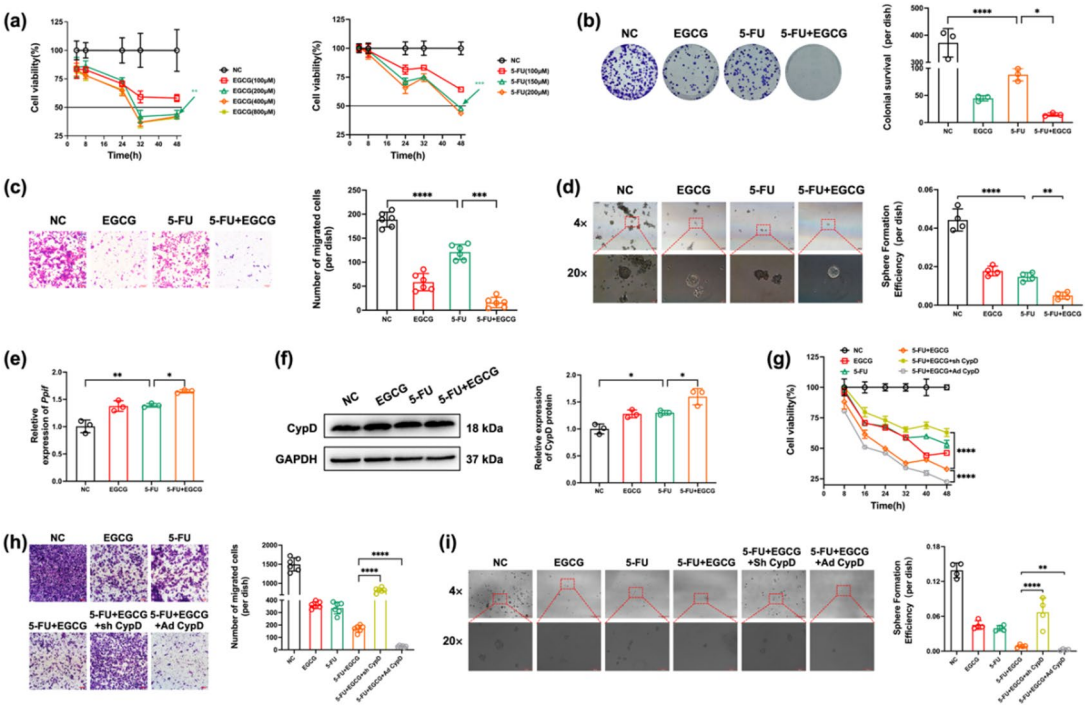

Fig. 5. CypD mediated the synergistic suppression of CRC cell malignant behaviors by EGCG and 5-FU. (**a**) Cell viability was assessed by CCK-8 after treating DLD1 cells with varying EGCG and 5-FU concentrations for different times (two-way ANOVA followed by Bonferroni-corrected *t*-test). (**b**) Colony formation ability was evaluated after 48 h treatment with EGCG (200 μM) and 5-FU (150 μM) (one-way ANOVA followed by Tukey's HSD test). (**c**) Cell migration assay was performed to analyze changes in DLD-1 cell motility under different treatments (scale bar = 100 μm; one-way ANOVA followed by Tukey's HSD test). (**d**) Self-renewal ability was assessed by spheroid formation assay (scale bar = 200 μm and 50 μm; one-way ANOVA followed by Tukey's HSD test). (**e**) *Ppif* gene expression was detected by RT-qPCR following various treatments (one-way ANOVA followed by Tukey's HSD test). (**f**) CypD protein expression was evaluated by Western blotting in DLD1 cells (one-way ANOVA followed by Tukey's HSD test). All Western blots were derived from physically cut membrane strips, and lanes non-adjacent or from different gels were separated by white space. (**g**) The effect of CypD knockdown or overexpression on cell viability under combined drug treatment was detected by CCK-8 (two-way ANOVA followed by Bonferroni-corrected *t*-test). (**h**–**i**) Migration ability and self-renewal capacity of DLD1 cells in each group were evaluated under same conditions as part g (one-way ANOVA followed by Tukey's HSD test). * $P<0.05$, ** $P<0.01$, *** $P<0.001$, and **** $P<0.0001$.

Discussion

In recent years, growing attention has been focused on the critical link between mitochondrial dysfunction and CRC pathogenesis[26–28]. CypD, a key mitochondrial matrix protein, plays a potential role in tumor cell apoptosis, oxidative stress, and energy metabolism by regulating mPT[8]. While limited studies (n = 4) have suggested that CypD inhibition may confer protective effects against chemotherapeutic agent-induced CRC cell death[15,16,29,30], its precise expression profile and specific regulatory mechanisms in CRC remain poorly characterized. Our study revealed significantly lower CypD expression levels in CRC tissues and cell lines compared to para-carcinoma tissues and normal colorectal epithelial cells. Knocking down CypD markedly enhanced CRC cells biological behaviors in vitro and tumorigenesis in vivo, whereas its overexpression produced opposing effects. Mechanistically, CypD promotes apoptosis in CRC cells through an autophagy-dependent pathway, as this process was effectively blocked by autophagy inhibitors. Furthermore, CypD upregulation significantly potentiates the synergistic inhibitory effects of EGCG and 5-FU on CRC cells. These findings suggest that enhancing CypD expression or function may represent a novel adjuvant approach for CRC management.

Although TCGA shows higher *Ppif* mRNA in T1 than in T4 lesions, this gradient is consistent with a progressive loss of CypD during CRC evolution. Early-stage tumors (T1) may retain high *Ppif* transcription levels contributed by immune or stromal cells, whereas advanced-stage tumors (T4) exhibit reduced intrinsic transcription coupled with enhanced post-transcriptional degradation (e.g., via miR-1281[31] and the ubiquitin-proteasome pathway). Thus, the downward trend from T1 to T4 reinforces the CRC-suppressive nature of CypD. Nevertheless, given the unequal sample sizes across stages in the TCGA dataset and the potential for post-transcriptional regulation, we therefore conducted the present study to definitively establish the role of CypD in CRC. Consistent with TCGA database analyses, RT-qPCR and IF staining revealed significantly reduced CypD mRNA and protein expression in CRC tissues compared to para-carcinoma tissues.

To characterize CypD's functional role in CRC progression, we conducted both loss-of-function and gain-of-function experiments. Notably, Ma et al. reported that CypD upregulation contributes to DN3-induced suppression of gastric cancer cell survival[32]. In alignment with these findings, CRC cells with CypD knockdown exhibited increased viability and colony formation, whereas CypD overexpression suppressed proliferation. However, we found that although RKO cells showed larger changes in *Ppif* mRNA and CypD protein levels upon genetic manipulation, the functional impact on cell proliferation was more pronounced in DLD1 cells. This discrepancy likely stems from cell-type-specific genetic backgrounds[23]. DLD1 cells harbor activating *KRAS* and *PI3K* mutations, which may synergize with CypD-mediated autophagy-apoptosis crosstalk to amplify growth inhibition. In contrast, RKO cells with microsatellite instability (MSI) and *BRAF* mutation may activate compensatory survival pathways (e.g., upregulation of Bcl-2 family proteins) that attenuate the proliferative consequences of CypD modulation. This was similar to the research results of Li et al.[33]. These findings highlight the complexity of CypD's role in CRC heterogeneity and suggest that therapeutic strategies targeting CypD may need to be tailored to specific molecular subtypes. Moreover, although mitochondrial functional changes due to CypD expression modulation might interfere with CCK-8 results, its consistency with findings from colony formation assays and apoptotic marker detection largely excludes potential confounding effects. Furthermore, Tavecchio et al. identified CypD as a critical effector in mitochondria-to-nuclei "retrograde" signaling that facilitates STAT3 and chemokine-dependent tumor cell motility[12]. Consistently, knocking down CypD accelerated CRC cell migration, whereas overexpression reduced it. However, it should be noted that prolonged cell migration assays may be confounded by concurrent cellular proliferation, particularly in cells that have transmigrated to the lower chamber. In future studies, we plan to employ live-cell imaging systems to dynamically track migratory trajectories, thereby minimizing interference from proliferative effects. Additionally, CypD downregulation enhanced CRC cell self-renewal capacity and xenograft tumor growth in nude mice, with opposing effects observed upon CypD overexpression. Shrestha et al. found that cyclosporine A (a CypD inhibitor) could significantly reverse the inhibitory effect of PF-543 on HCT-116 xenografts growth[15], supporting our findings. Overall, these results strongly indicate that CypD may suppress CRC development.

CypD is well-established to mediate the initiation of apoptotic pathways by enhancing mPT[34]. Its upregulation is linked to apoptosis induced by multiple chemotherapeutic drugs[35,36]. For instance, DN3 induces apoptosis in gastric cancer cells by upregulating CypD[32]. Based on these findings, this study mainly evaluated CypD's impact on CRC cell apoptosis. Results indicated that knocking down CypD significantly suppressed pro-apoptotic gene expression (Bax and Cleaved-Caspase 3) while enhancing anti-apoptotic Bcl-2 expression, with opposing effects observed following CypD overexpression. Based on the decreased Bcl-2/Bax ratio and upregulated Cleaved-Caspase3, along with the known function of CypD, it is inferred that apoptosis is triggered via the mitochondrial pathway. Moreover, given the highly significant differences in the changes of the apoptotic marker Cleaved-Caspase3 across groups following CypD expression modulation (both $P < 0.0001$), it is suggested that cell death may be the primary cause of the decline in cell viability. In parallel, drug-induced CypD elevation has been shown to trigger autophagy in hepatocellular carcinoma[37]. This study demonstrated that knocking down CypD inhibits CRC cell autophagy, whereas CypD overexpression promotes it. Given that autophagy can modulate apoptosis via caspases and other pro-apoptotic proteins as intermediary participants[38], we hypothesized that CypD promotes apoptosis by regulating autophagy. To verify this hypothesis, the autophagy inhibitor CQ was employed and significantly reversed the apoptosis induced by CypD overexpression. Critically, CQ not only eliminated the differences in the expression of apoptotic and autophagic markers between CypD-overexpressing cells and control cells but also induced a "net reduction" of the LC3-II/I ratio in CQ-Ad CypD group. These results demonstrate that CypD's pro-apoptotic effect is strictly dependent on intact autophagic flux. Moreover, CQ exhibited comparable inhibitory effects on CRC cell apoptosis regardless of CypD expression status. Although a 24-hour CQ treatment revealed significant autophagy blockade, various time points and CRISPR-based knockdown of essential autophagy genes (such as ULK1 complex and ATG5) are required in the future to establish the kinetics and genetic dependency of CypD-driven autophagy-apoptosis crosstalk. We also anticipate providing ultrastructural and single-cell evidence through high-resolution imaging in future studies. Collectively, this provides new insights into the molecular mechanism linking CypD to CRC progression and highlights the potential of targeting the CypD-autophagic flux axis for CRC therapy.

As a first-line chemotherapeutic agent for CRC, 5-FU demonstrates significantly enhanced antitumor efficacy when combined with EGCG[21]. Studies have shown that combinatorial treatment with 5-FU and gambogenic acid exerts cytotoxicity in lung cancer cells through CypD upregulation[18]. EGCG also suppressed the growth of salivary adenoid cystic carcinoma cells by activating mitochondrial apoptosis pathways[39]. Notably, to the best of our knowledge, no previous studies have linked CypD to the synergistic antitumor effect of EGCG and 5-FU in CRC. This is the first report to identify CypD as a key mediator of this synergy. To address this knowledge gap, we first observed that combination therapy elevated CypD expression in CRC cells. Cell function experiments subsequently showed that CypD knockdown protected CRC cells from the toxicity of this combination, while CypD overexpression had the opposite effect. These findings suggest that CypD may play a pivotal role in the synergistic inhibition of CRC progression by EGCG and 5-FU, potentially serving as a predictive biomarker for combination therapy. Patients with higher intrinsic CypD expression are likely to derive greater benefit from this regimen, whereas those with low CypD levels may exhibit reduced responsiveness. Additionally, targeting CypD (e.g., via pharmacological activators) could enhance chemotherapeutic efficacy, particularly in chemoresistant CRC subtypes. These hypotheses warrant validation through future preclinical and clinical investigations.

While this study provides critical insights into CypD's role in CRC progression and therapeutic response, several knowledge gaps remain to be addressed. Firstly, recent studies have hinted at potential upstream regulators of CypD in CRC, although their mechanisms remain incompletely elucidated. For example, mitochondrial chaperone TRAP1 was overexpressed in CRC and could prevent CypD translocation and pro-apoptotic activity[40]. The peptide encoded by circp53 (circp53-209aa) competitively bound to CypD, dissociating it from

the CypD/TRAP1/HSP90 complex[29]. SIRT3 could also modulate CypD activity through deacetylation, thereby influencing glycolysis in CRC[30]. These upstream regulators (TRAP1, circp53, SIRT3) offer potential therapeutic avenues for restoring CypD function. Future investigations could explore their crosstalk with the autophagy-apoptosis pathway identified in our study, which would clarify whether synergistic targeting of CypD and its upstream network can enhance the efficacy of CRC therapies. Moreover, CypD is crucial in mitochondria-to-nuclei interorganelle signaling. Its reduced expression could enhance the malignancy of various cancer cells via Cxcl12-Cxcr4-directed chemotaxis[12]. However, whether there are similar extramitochondrial pathways in the inhibitory effect of CypD on CRC still requires in-depth analysis. Meanwhile, to more comprehensively capture the heterogeneity of CRC, in the future, we will further validate the broad applicability of the findings of this study in other CRC models (such as CRC cell lines with distinct molecular characteristics or patient-derived xenografts) and in a larger cohort of CRC patients (such as large-scale tissue microarrays).

Conclusions

In summary, we demonstrated that CypD is downregulated in CRC. Knocking down CypD significantly increased CRC cell proliferation, migration, and subcutaneous tumor growth, whereas its overexpression produced the opposite effects. Mechanistically, CypD promoted apoptosis through autophagy activation in CRC cells, and this process could be blocked by autophagy inhibitors. Furthermore, CypD facilitated the synergistic inhibition of CRC cells by EGCG and 5-FU. These findings suggest that therapeutic potentiation of CypD may serve as a novel adjuvant strategy for CRC treatment by promoting autophagy-mediated apoptosis to suppress tumor progression.

Materials and methods

Tissue samples

Cancerous and para-carcinoma tissues were collected from 13 patients who underwent surgical resection for CRC at the Affiliated Hospital of Jining Medical University from March 2022 to October 2023. All participants provided written informed consent and had no history of preoperative radiotherapy or chemotherapy. This study was approved by the Medical Research Ethics Committee of the Affiliated Hospital of Jining Medical University (No. 2021B052) and strictly adhered to the Declaration of Helsinki. For 11 patients, total RNA was extracted from both CRC and para-carcinoma tissues to analyze *Ppif* gene expression via real-time quantitative polymerase chain reaction (RT-qPCR). Paraffin-embedded sections were prepared from the remaining 2 cases for immunofluorescence (IF) staining to evaluate CypD protein expression in paired cancerous and para-carcinoma tissues.

Cell culture, lentiviral transfection and drug treatment

Human colorectal cancer cell lines (DLD-1, RKO, HCT116) and the human normal colorectal epithelial cell line NCM460 were kindly provided by Associate Researcher Baoyu He from the Affiliated Hospital of Jining Medical University. NCM460 and HCT116 cells were cultured in Dulbecco's Modified Eagle Medium (DMEM; Gibco) supplemented with 10% fetal bovine serum (FBS; Gibco, Thermo Fisher Scientific, MA, USA) and 1% penicillin/streptomycin (P/S; Solarbio, Beijing, China). DLD-1 and RKO cells were maintained in Roswell Park Memorial Institute (RPMI) 1640 medium (Gibco) containing 10% FBS and 1% P/S. All cell lines were incubated in a humidified atmosphere with 5% CO_2 at 37 °C.

The lentiviral vectors expressing shRNA targeting human *Ppif* (target sequence: 5'-GAATCTTTCGGCTC TAAGAG-3') and lentivirus encoding human *Ppif*-EGFP were purchased from Obio Technology (Shanghai, China). The well-conditioned CRC cells were seeded in 24-well plates at 5×10^4 cells/well and cultured to 40% confluency. Subsequently, lentivirus at optimal dilution was transfected into CRC cells using 6 μg/mL polybrene solution (Obio) according to the manufacturer's instructions. After 20 h of transfection, the medium was replaced with regular complete medium, and the cells were continuously cultured. At 72 h post-infection (Day 3), the transfection efficiency was evaluated under a fluorescence microscope, with > 80% GFP^+ cells considered qualified for subsequent antibiotic selection. Multiple rounds of puromycin (Biosharp, Anhui, China) selection with escalating concentrations were performed to establish stably transfected cell lines, following this exact schedule: (1) Day 3–5 (post-infection): Cells were cultured in medium containing 2.5 μg/mL puromycin for 1–2 days, then transferred to regular medium and cultured until reaching 80%–90% confluency. (2) Day 5–8 (post-infection): Cells were cultured in medium containing 5 μg/mL puromycin for 1–2 days, then again cultured in regular medium until 80%–90% confluency. (3) Day 8–11 (post-infection): Cells were cultured in medium containing 10 μg/mL puromycin for 1–2 days, followed by recovery in drug-free medium for 2–3 days. (4) Day 11–15 (post-infection): When cells expanded in 10 cm dishes reached 80%-90% confluency, total RNA and protein were harvested for the first validation of CypD expression (knockdown/overexpression efficiency). Subsequent maintenance screenings were carried out every 15–20 days using complete medium supplemented with 10 μg/mL puromycin to ensure the transfection efficiency. All subsequent functional and xenograft assays were initiated within 1–5 passages after this first validation.

Working solutions of these agents were prepared according to the manufacturer's protocol. Stably transfected CRC cell lines were treated with the autophagy inhibitor CQ (100 μM; GLPBIO, CA, USA), 5-FU (100, 150, 200 μM; GLPBIO), or EGCG (100, 200, 400 μM; GLPBIO) following the experimental protocol.

RT-qPCR

Fresh tissues snap-frozen in liquid nitrogen were rapidly transferred to a mortar pre-cooled with liquid nitrogen and ground to a fine powder. The powder was then collected into a 1.5 mL RNase-free tube. Drug-treated or lentivirus-infected CRC cells were dissociated with trypsin, washed once with ice-cold RNase-free ddH_2O, and

pelleted by centrifugation at 1000 × g for 5 min at 4°C. Subsequently, samples (about 25 mg tissue or 1–5 × 10^6 CRC cells) were completely lysed in 500 μL RNA-easy Isolation Reagent (Vazyme, Nanjing, China) and homogenized thoroughly. To the above lysates, 100 μL chloroform (Sangon Biotech, Shanghai, China) was added, vortexed vigorously for 15 seconds, and incubated on ice for 5 min. The mixture was centrifuged at 12,000 × g for 15 min at 4°C, and the upper aqueous phase (containing RNA) was carefully transferred to a new RNase-free tube. Total RNA was then extracted according to the manufacturer's instructions without modification. RNA concentration was measured with a NanoDrop 2000 spectrophotometer (Thermo Fisher Scientific), and purity was assessed by the OD260/OD280 ratio (1.8–2.0 considered qualified). The HiScript III RT SuperMix for qPCR (+gDNA wiper) (Vazyme) was used to reverse transcribe mRNA into cDNA according to the manufacturer's instructions. qPCR was performed on a QuantStudio 5 Real-Time PCR System (Applied Biosystems, MA, USA) with ChamQ SYBR qPCR Master Mix (Vazyme) with the given thermal cycling conditions according to the manufacturer's instructions. Primer sequences (Sangon Biotech, Shanghai, China) were as follows: *Ppif* (F: 5'-ACAGGCGGGA AGTCCATCTACG-3'; R: 5'-GAACTGGGAGCCGTTGGTGTTAG-3') and *β-actin* (F: 5'-GACCTGTACGCCA ACACAGT-3'; R: 5'-CTCAGGAGGAGCAATGATCT-3'). Relative *Ppif* expression levels were normalized to the housekeeping gene *β-actin* using the $2^{-\Delta\Delta CT}$ method.

IF staining

Paraffin-embedded sections of CRC tissues were deparaffinized in deparaffinizing solution (3 × 10 min; Solarbio) and rehydrated through graded ethanol (100% → 95% → 70%, 5 min each; Shuangshuang, Shandong, China). Antigen retrieval was performed by microwave heating in Tris-EDTA buffer (Solarbio) for 15 min, followed by cooling to room temperature. Endogenous peroxidase activity was quenched with 3% H_2O_2 for 10 min, and sections were blocked with 5% BSA (Biosharp) for 30 min at room temperature. Sections were incubated with primary rabbit anti-CypD antibody (1:150, Abcam, Cambridge, UK; Cat# ab231155) overnight at 4 °C in a humidified chamber. After washing with 1×TBST (3 × 3 min), sections were incubated with HRP-conjugated mouse/rabbit cross-reactive secondary antibody (from four-color multiplex fluorescence IHC kit, Absin, Shanghai, China; Cat# abs50012) for 30 min at room temperature in the dark. Following 1×TBST washes (3 × 3 min), 1× TSA520 working solution (diluted in kit-provided signal amplification buffer at 1:100) was added and incubated for 10 min at room temperature in the dark to visualize CypD (green fluorescence). Sections were then washed with 1×TBST (3 × 3 min), and nuclei were counterstained with 1× DAPI (provided in the kit) for 5 min at room temperature. After washing with 1×TBST (3 × 2 min), anti-fluorescence quenching mounting medium (provided in the kit) was added, and the edges of the coverslip were sealed with clear nail polish. Fluorescence images were captured using a ZEISS LSM 800 confocal microscope (20× magnification) and quantified with ImageJ software (National Institutes of Health, MD, USA).

Western blotting

Total protein was extracted from CRC tissues and cells using RIPA lysis buffer (Beyotime, Shanghai, China) supplemented with 1× protease inhibitor (GLPBIO). Samples were lysed on ice for 30 min with intermittent vortexing, then centrifuged at 12,000 × g for 15 min at 4 °C. The supernatant was collected as total protein extract, and protein concentration was measured with a BCA Protein Assay Kit (GLPBIO). Equal protein amounts (20 μg/lane) were loaded alongside 3 μL of protein ladder (PageRuler, Thermo Fisher Scientific). Proteins were separated on 10% or 12.5% SDS-PAGE gels for those above 70 kDa or below 30 kDa, respectively. Separated proteins were transferred to 0.22 μm polyvinylidene fluoride (PVDF) membranes (Bio-Rad, Hercules, USA) via wet transfer. After transfer, membranes were blocked with 5% skim milk (Beyotime) in 1 × TBST for 1.5 h at room temperature. Membranes were then incubated with primary antibodies (diluted in 5% BSA/TBST) overnight at 4 °C on a rocking platform. Following washing and rewarming, membranes were incubated with HRP-conjugated secondary antibodies (diluted in 5% BSA/TBST) for 1 h at room temperature. Immunoreactive bands were visualized using a ECL chemiluminescence kit (Vazyme) and quantified with ImageJ software and normalized to the internal reference protein GAPDH. All antibody details are provided in Table 1.

Cell viability assay

CRC cells were seeded into 96-well plate at 2 × 10^3 cells/well and cultured under standard conditions. At designated time points, 20 μL CCK-8 reagent (GLPBIO) was added to each well following experimental protocol. After incubation at 37 °C for 2 h, the plate was shaken for 1 min and the absorbance at 450 nm was measured using a Synergy H1 Multimode Reader (BioTek, Vermont, USA). The absorbance values obtained at each time point were used to plot the cell growth curve.

Colony formation assay

CRC cells were seeded into six-well plate at 2 × 10^3 cells/well and cultured until visible colonies formed after about two weeks. Cultures were terminated by fixation with 4% paraformaldehyde (PAF; Biosharp) at 2 mL/well for 20 min, followed by staining with 0.1% crystal violet solution (Leagene, Beijing, China) at 1 mL/well for 30 min. Colonies were photographed and quantified using an IM-300 inverted microscope (OPTIKA, Milan, Italy).

Cell migration assay

CRC cells in logarithmic growth phase were trypsinized and resuspended in serum-free RPMI 1640 medium to achieve a final concentration of 1 × 10^6 cells/mL. 200 μL cell suspension was added to the upper chamber of transwell inserts (6.5 mm diameter, 8.0 μm pore size; Corning, NY, USA), while the lower chamber was filled with 1 mL of complete medium containing 20% FBS and 1% P/S. Following 48–72 h incubation, inserts were gently rinsed, fixed with 4% PAF for 20 min, and stained with 0.1% crystal violet solution for 30 min. Non-

Antibodies	Source	Dilution ratio	Manufacturer
GAPDH	Mouse	1:10000	Bioworld Technology (Cat# AP0063; RRID: AB_2651132)
CypD	Rabbit	1:5000	Abcam (Cat# ab231155)
Bcl-2	Rabbit	1:1000	Proteintech (Cat# 12789-1-AP, RRID: AB_2227948)
Bax	Rabbit	1:1000	Proteintech (Cat# 50599-2-Ig, RRID: AB_2061561)
Cleaved-Caspase 3	Rabbit	1:1000	Cell Signaling Technology (Cat# 9661, RRID: AB_2341188)
p62	Mouse	1:1000	Cell Signaling Technology (Cat# 66277; RRID: AB_2890160)
ATG5	Rabbit	1:1000	Cell Signaling Technology (Cat# 12994; RRID: AB_2630393)
ATG7	Rabbit	1:1000	Cell Signaling Technology (Cat# 2631; RRID: AB_2227783)
LC3	Rabbit	1:1000	Cell Signaling Technology (Cat# 4108; RRID: AB_2137703)
Anti-rabbit IgG-HRP	Goat	1:3000	Cell Signaling Technology (Cat# 7074; RRID: AB_2099233)
Anti-mouse IgG-HRP	Horse	1:3000	Cell Signaling Technology (Cat# 7076; RRID: AB_330924)

Table 1. Antibodies information.

migrated cells in the upper chamber were carefully removed using cotton swabs, followed by air-dried. The inserts were placed on slides, and images were captured at 10× magnification using an inverted microscope.

Spheroid formation assay

Cells from each group were trypsinized and seeded into ultra-low attachment six-well plate (Corning) at 2×10^3 cells/well. Cultures were maintained in serum-free RPMI 1640 medium supplemented with 20 ng/mL EGF (Gibco), 10 ng/mL bFGF (Gibco), 2% B27 (Gibco), and 1% P/S. After 10–14 days of incubation, cultures were terminated when macroscopic spheroids became visible. Spheroid numbers were counted and images were taken under an inverted microscope at 4× and 20× magnification. Spheroid formation efficiency (SFE) was calculated to evaluate self-renewal capacity using the formula: SFE (%) = (number of spheroids / initial cell number) × 100.

In vivo tumor xenograft model

Male BALB/c nude mice (age: 6–8 weeks, weight: about 17 g) were purchased from Jinan Pengyue Experimental Animal Breeding Co., Ltd. (License No. SCXK (Lu) 2022 0006, Shandong, China). Mice ($n = 3$/cage) were housed under specific pathogen-free (SPF) conditions at Jining Medical University (25 °C, 55% humidity, 12 h light/dark cycle) with free access to food and water. Mice were randomly into four groups ($n = 6$/group): sh NC, sh CypD, Ad vector, and Ad CypD. To minimize confounders, all experimental procedures were performed by the same researcher following standardized protocols to ensure consistency. All mice were housed under identical environmental conditions to mitigate positional effects. After one week of adaptation, according to the group arrangement, 200 μL DLD1 cell suspension (5×10^6 cells) of the corresponding group was subcutaneously injected into the right axilla of each mouse following the protocol described by Yang et al.[41]. Tumor dimensions were measured weekly using calipers, and volumes were calculated using the formula: volume = (length × width^2)/2. Growth curves were plotted based on five consecutive weeks of measurements.

Mice were euthanized prior to the experimental endpoint if they exhibited: (1) tumor volume exceeding 2,000 mm^3 (calculated weekly); (2) ulceration or necrosis of the tumor; (3) significant weight loss (> 20% of initial body weight); (4) persistent lethargy or impaired mobility. In this study, the above situation did not occur and all mice completed the full analytical protocol. On day 23 post-injection, mice were euthanized via anesthesia with 3% isoflurane followed by cervical dislocation. Death was confirmed through secondary verification of cardiac arrest prior to tumor excision, weighing, and photographic documentation. No surviving mice were found after the experiment. Some tumors were paraffin-embedded for immunohistochemical (IHC) staining and others were stored in liquid nitrogen for Western blotting. All procedures were approved by the Medical Research Ethics Committee of the Affiliated Hospital of Jining Medical University (No. 2021B052) and were conducted following the ARRIVE guidelines.

IHC staining

Paraffin-embedded subcutaneous tumor Sect. (4 μm thick) were deparaffinized with deparaffinization solution (3 × 7 min) and rehydrated by gradient ethanol (100% → 95% → 70%, 5 min each), followed by rinsing. Antigen retrieval was performed by microwave heating in 1× citrate antigen retrieval solution (pH 6.0; Biosharp) at 95 °C for 15 min, followed by natural cooling to room temperature. Sections were then immersed in 3% H_2O_2 (Anyongbo, Fujian, China) for 15 min to block endogenous peroxidase activity. After washing with 1×PBS (3 × 1 min), 5% BSA was added, and the sections were incubated at room temperature with gentle shaking for

30 min. Sections were incubated with rabbit anti-Ki67 primary antibody (1:500; ABclonal, Wuhan, China; Cat# A20018; RRID: AB_3065688) overnight at 4 °C in a dark chamber. The following day, sections were washed with 1×PBS (3×3 min) and incubated with HRP-conjugated mouse/rabbit cross-reactive secondary antibody (from four-color multiplex fluorescence IHC kit as set forth) for 30 min at room temperature. DAB (Proteintech, Wuhan, China) was applied for 1 min to visualize immunoreactivity (monitored under a microscope to avoid overstaining), followed by hematoxylin counterstaining (Beyotime) for 3 min. Sections were dehydrated through gradient ethanol (70% → 95% → 100%, 5 min each) and immersed in deparaffinization buffer (3×5 min). Finally, sections were mounted with neutral balsam (Beyotime) and observed under a light microscope.

Statistical analysis

Data are presented as mean ± standard deviation. The specific statistical analysis methods are described as follows: Comparisons of CypD protein expression differences between T1 and T4 stage CRC tissues from the TCGA database (Fig. 1a) were performed using the Mann-Whitney *U* test. Analysis of *Ppif* gene expression differences between CRC tissues and para-carcinoma tissues in clinical samples (Fig. 1c) was conducted with the paired *t*-test. All other pairwise comparisons were performed using independent-samples *t*-test. For multiple group comparisons, one-way analysis of variance (ANOVA) followed by Tukey's honest significant difference (HSD) test was used for time-independent analyses, while two-way ANOVA followed by Bonferroni-corrected *t*-test was applied for time-dependent multiple group comparisons. Data normality was verified by the Shapiro-Wilk test. $P < 0.05$ was considered statistically significant.

Data availability

Data is provided within the manuscript.

Received: 7 October 2025; Accepted: 22 December 2025
Published online: 26 December 2025

References

1. Bray, F. et al. Global cancer statistics 2022: GLOBOCAN estimates of incidence and mortality worldwide for 36 cancers in 185 countries. *CA Cancer J. Clin.* **74**, 229–263 (2024).
2. Eng, C. et al. *Colorectal Cancer Lancet* **404**, 294–310 (2024).
3. Li, F. et al. Molecular targeted therapy for metastatic colorectal cancer: current and evolving approaches. *Front. Pharmacol.* **14**, 1165666 (2023).
4. Zhou, S., Yu, Q., Zhang, L. & Jiang, Z. Cyclophilin D-mediated mitochondrial permeability transition regulates mitochondrial function. *Curr. Pharm. Des.* **29**, 620–629 (2023).
5. Protasoni, M. et al. Cyclophilin D plays a critical role in the survival of senescent cells. *Embo J.* **43**, 5972–6000 (2024).
6. Ikeda, G. et al. Nanoparticle-Mediated simultaneous targeting of mitochondrial injury and inflammation attenuates myocardial Ischemia-Reperfusion injury. *J. Am. Heart Assoc.* **10**, e019521 (2021).
7. Samanta, S. et al. New Cyclophilin D inhibitor rescues mitochondrial and cognitive function in alzheimer's disease. *Brain* **147**, 1710–1725 (2024).
8. Zhang, L. et al. Cyclophilin D: guardian or executioner for tumor cells? *Front. Oncol.* **12**, 939588 (2022).
9. Wen, M. et al. Design, Synthesis, and biological evaluation of Esculetin-Furoxan-DEAC ternary hybrids for Anti-Triple negative breast cancer. *J. Med. Chem.* **66**, 12446–12458 (2023).
10. Wu, P. K., Hong, S. K. & Park, J. I. Mortalin depletion induces MEK/ERK-dependent and ANT/CypD-mediated death in vemurafenib-resistant B-Raf(V600E) melanoma cells. *Cancer Lett.* **502**, 25–33 (2021).
11. Pan, H., Wang, B. H., Lv, W., Jiang, Y. & He, L. Esculetin induces apoptosis in human gastric cancer cells through a Cyclophilin D-mediated mitochondrial permeability transition pore associated with ROS. *Chem. Biol. Interact.* **242**, 51–60 (2015).
12. Tavecchio, M. et al. Cyclophilin D extramitochondrial signaling controls cell cycle progression and chemokine-directed cell motility. *J. Biol. Chem.* **288**, 5553–5561 (2013).
13. Ghosh, J. C. et al. Adaptive mitochondrial reprogramming and resistance to PI3K therapy. *J. Natl. Cancer Inst.* **107**, dju502 (2015).
14. Huo, H. et al. Erastin disrupts mitochondrial permeability transition pore (mPTP) and induces apoptotic death of colorectal cancer cells. *PLoS One.* **11**, e0154605 (2016).
15. Ju, T., Gao, D. & Fang, Z. Y. Targeting colorectal cancer cells by a novel sphingosine kinase 1 inhibitor PF-543. *Biochem. Biophys. Res. Commun.* **470**, 728–734 (2016).
16. Zhou, C. et al. Icaritin activates JNK-dependent mPTP necrosis pathway in colorectal cancer cells. *Tumour Biol.* **37**, 3135–3144 (2016).
17. Valencia-Lazcano, A. A. et al. 5-Fluorouracil nano-delivery systems as a cutting-edge for cancer therapy. *Eur. J. Med. Chem.* **246**, 114995 (2023).
18. Su, J. et al. Synergistic effects of 5-fluorouracil and gambogenic acid on A549 cells: activation of cell death caused by apoptotic and necroptotic mechanisms via the ROS-mitochondria pathway. *Biol. Pharm. Bull.* **37**, 1259–1268 (2014).
19. Wang, L., Li, P. & Feng, K. EGCG adjuvant chemotherapy: current status and future perspectives. *Eur. J. Med. Chem.* **250**, 115197 (2023).
20. Zhou, M. et al. Chitosan-Gelatin-EGCG Nanoparticle-Meditated LncRNA TMEM44-AS1 Silencing to activate the P53 signaling pathway for the synergistic reversal of 5-FU resistance in gastric cancer. *Adv. Sci.* **9**, e2105077 (2022).
21. La, X., Zhang, L., Li, Z., Li, H. & Yang, Y. -)-Epigallocatechin gallate (EGCG) enhances the sensitivity of colorectal cancer cells to 5-FU by inhibiting GRP78/NF-κB/miR-155-5p/MDR1 pathway. *J. Agric. Food Chem.* **67**, 2510–2518 (2019).
22. Wu, A. et al. (-)-Epigallocatechin-3-gallate directly binds Cyclophilin D: A potential mechanism for mitochondrial protection. *Molecules* **27**, 8661 (2022).
23. Zheng, C. C. et al. Blockade of nuclear β-Catenin signaling via direct targeting of RanBP3 with NU2058 induces cell senescence to suppress colorectal tumorigenesis. *Adv. Sci.* **9**, e2202528 (2022).
24. Sorice, M. Crosstalk of autophagy and apoptosis. *Cells* **11**, 1479 (2022).
25. Cocco, S. et al. Inhibition of autophagy by chloroquine prevents resistance to PI3K/AKT inhibitors and potentiates their antitumor effect in combination with Paclitaxel in triple negative breast cancer models. *J. Transl Med.* **20**, 290 (2022).
26. Jackson, D. N. & Theiss, A. L. Gut bacteria signaling to mitochondria in intestinal inflammation and cancer. *Gut Microbes.* **11**, 285–304 (2020).
27. Wu, Z. et al. Mitochondrial dynamics and colorectal cancer biology: mechanisms and potential targets. *Cell. Commun. Signal.* **22**, 91 (2024).

28. Haque, P. S., Kapur, N., Barrett, T. A. & Theiss, A. L. Mitochondrial function and Gastrointestinal diseases. *Nat. Rev. Gastroenterol. Hepatol.* **21**, 537–555 (2024).
29. Yu, X. et al. Extracellular vesicle-mediated delivery of circp53 suppresses the progression of multiple cancers by activating the CypD/TRAP/HSP90 pathway. *Exp. Mol. Med.* **57**, 1711–1726 (2025).
30. Liu, Z., Li, L. & Xue, B. Effect of Ganoderic acid D on colon cancer Warburg effect: role of SIRT3/cyclophilin D. *Eur. J. Pharmacol.* **824**, 72–77 (2018).
31. Jia, J., Xia, J., Liu, W., Tao, F. & Xiao, J. Cinnamtannin B-1 inhibits the progression of osteosarcoma by regulating the miR-1281/PPIF axis. *Biol. Pharm. Bull.* **46**, 67–73 (2023).
32. Ma, Y. C. et al. A novel ent-kaurane diterpenoid analog, DN3, selectively kills human gastric cancer cells via acting directly on mitochondria. *Eur. J. Pharmacol.* **848**, 11–22 (2019).
33. Li, G., Li, B., Song, J., Wang, N. & Gao, Z. Endomorphin-2 analog inhibits the growth of DLD-1 and RKO human colon cancer cells by inducing cell apoptosis. *Med. Sci. Monit.* **26**, e921251 (2020).
34. Hong, K., Yang, Q., Liu, G., Qiu, H. & Yu, B. Cyclophilin D regulates oxidative stress and apoptosis via mitochondrial permeability transition pore in acute acalculous cholecystitis. *Curr. Mol. Med.* **23**, 971–980 (2023).
35. Hou, D. et al. Cationic antimicrobial peptide NRC-03 induces oral squamous cell carcinoma cell apoptosis via CypD-mPTP axis-mediated mitochondrial oxidative stress. *Redox Biol.* **54**, 102355 (2022).
36. Hu, W. et al. Cyclophilin D-mediated apoptosis attributes to sorafenib-induced cytotoxicity in clear cell-renal cell carcinoma. *Eur. J. Pharmacol.* **749**, 142–150 (2015).
37. Chen, W., Feng, L., Nie, H. & Zheng, X. Andrographolide induces autophagic cell death in human liver cancer cells through Cyclophilin D-mediated mitochondrial permeability transition pore. *Carcinogenesis* **33**, 2190–2198 (2012).
38. Sun, D. et al. Trifolirhizin induces autophagy-dependent apoptosis in colon cancer via AMPK/mTOR signaling. *Signal. Transduct. Target. Ther.* **5**, 174 (2020).
39. Weng, L. X., Wang, G. H., Yao, H., Yu, M. F. & Lin, J. Epigallocatechin gallate inhibits the growth of salivary adenoid cystic carcinoma cells via the EGFR/Erk signal transduction pathway and the mitochondria apoptosis pathway. *Neoplasma* **64**, 563–570 (2017).
40. Zhao, K. et al. An orally administered gene editing nanoparticle boosts chemo-immunotherapy in colorectal cancer. *Nat. Nanotechnol.* **20**, 935–946 (2025).
41. Yang, J. et al. Cetuximab promotes RSL3-induced ferroptosis by suppressing the Nrf2/HO-1 signalling pathway in KRAS mutant colorectal cancer. *Cell. Death Dis.* **12**, 1079 (2021).

Acknowledgements
We are grateful to the members of the Bin Zhang Lab at the Affiliated Hospital of Jining Medical University for their support throughout this study. Meanwhile, the authors especially thank the CRC patients who participated in this study.

Author contributions
Ling Zhang: Conceptualization, Validation, Writing – original draft., Visualization, Funding acquisition. Yi Liu: Conceptualization, Methodology, Validation, Visualization. Ruiqi Liu: Methodology, Data curation, Formal analysis. Wenjun Wang: Supervision, Formal analysis, Writing – review & editing. Ruiji Li: Supervision, Writing – review & editing, Funding acquisition. All authors have read and approved the manuscript.

Funding
This study was funded by the Natural Science Foundation of Shandong Province (ZR2021QH294; ZR2021QB124), Research Fund for Academician Lin He New Medicine (JYHL2022MS02) and Outstanding Youth Foundation (Overseas) Project of Rizhao City Natural Science Foundation (RZ2021ZR1).

Declarations

Competing interests
The authors declare no competing interests.

Ethics approval and consent to participate
This study involving CRC patients and node mice were approved by the Medical Research Ethics Committee of the Affiliated Hospital of Jining Medical University (No. 2021B052). And this study was performed in line with the principles of the Declaration of Helsinki and the ARRIVE guidelines. Informed consent was obtained from all individual participants included in the study.

Additional information
Supplementary Information The online version contains supplementary material available at https://doi.org/10.1038/s41598-025-33774-1.

Correspondence and requests for materials should be addressed to W.W. or R.L.

Reprints and permissions information is available at www.nature.com/reprints.

Publisher's note Springer Nature remains neutral with regard to jurisdictional claims in published maps and institutional affiliations.

Open Access This article is licensed under a Creative Commons Attribution-NonCommercial-NoDerivatives 4.0 International License, which permits any non-commercial use, sharing, distribution and reproduction in any medium or format, as long as you give appropriate credit to the original author(s) and the source, provide a link to the Creative Commons licence, and indicate if you modified the licensed material. You do not have permission under this licence to share adapted material derived from this article or parts of it. The images or other third party material in this article are included in the article's Creative Commons licence, unless indicated otherwise in a credit line to the material. If material is not included in the article's Creative Commons licence and your intended use is not permitted by statutory regulation or exceeds the permitted use, you will need to obtain permission directly from the copyright holder. To view a copy of this licence, visit http://creativecommons.org/licenses/by-nc-nd/4.0/.

© The Author(s) 2025